Septins 2, 7 and 9 and MAP4 colocalize along the axoneme in the primary cilium and control ciliary length

Rania Ghossoub[1,2,3], Qicong Hu[4], Marion Failler[1,2,3,5], Marie-Christine Rouyez[1,2,3], Benjamin Spitzbarth[6], Serge Mostowy[7,8,9,*], Uwe Wolfrum[6], Sophie Saunier[3,5], Pascale Cossart[7,8,9], W. James Nelson[4,10,‡,§] and Alexandre Benmerah[1,2,3,5,‡,§]

[1]INSERM U1016, Insitut Cochin, Paris, France
[2]CNRS UMR8104, Paris, France
[3]Université Paris Descartes, Sorbonne Paris Cité, Institut Imagine, Paris, France
[4]Department of Biology, Stanford University, Stanford, CA, USA
[5]INSERM, U983, Hôpital Necker-Enfants Malades, Paris, France
[6]Department of Cell and Matrix Biology, Institute of Zoology, Johannes Gutenberg University, Mainz, Germany
[7]Institut Pasteur, Unité des Interactions Bactéries-Cellules, Département de Biologie Cellulaire et Infection, Paris, France
[8]INSERM, U604, Paris, France
[9]INRA, USC2020, Paris, France
[10]Department of Molecular and Cellular Physiology, Stanford University, Stanford, CA, USA

*Present address: Section of Microbiology, MRC Centre for Molecular Bacteriology and Infection, Imperial College London, London, UK
‡These authors contributed equally to this work
§Authors for correspondence (wjnelson@stanford.edu; alexandre.benmerah@inserm.fr)

Accepted 20 March 2013
Journal of Cell Science 126, 2583–2594

doi: 10.1242/jcs.111377

Summary

Septins are a large, evolutionarily conserved family of GTPases that form hetero-oligomers and interact with the actin-based cytoskeleton and microtubules. They are involved in scaffolding functions, and form diffusion barriers in budding yeast, the sperm flagellum and the base of primary cilia of kidney epithelial cells. We investigated the role of septins in the primary cilium of retinal pigmented epithelial (RPE) cells, and found that SEPT2 forms a 1:1:1 complex with SEPT7 and SEPT9 and that the three members of this complex colocalize along the length of the axoneme. Similar to observations in kidney epithelial cells, depletion of cilium-localized septins by siRNA-based approaches inhibited ciliogenesis. MAP4, which is a binding partner of SEPT2 and controls the accessibility of septins to microtubules, was also localized to the axoneme where it appeared to negatively regulate ciliary length. Taken together, our data provide new insights into the functions and regulation of septins and MAP4 in the organization of the primary cilium and microtubule-based activities in cells.

Key words: Primary cilium, Septins, MAP4, Microtubules, Actin

Introduction

Septins are a highly conserved family of small GTPases that form hetero-oligomers that assemble into filaments, rings and spirals. Originally, septins were identified as important regulators of cytokinesis in organisms ranging from yeast to mammals. In yeast, septins assemble at the neck between the mother and daughter bud into interlocking rings that form a barrier to the lateral diffusion of proteins and mRNAs from the mother to the daughter cell, and a scaffold for the assembly of the contractile ring. In mammals, septins localize to the cleavage furrow and midbody, and perturbation of septin functions leads to cytokinesis defects (reviewed by Saarikangas and Barral, 2011; Mostowy and Cossart, 2012).

In mammals, septins have been linked to scaffolding functions with the cytoskeleton. In most cells, septins colocalize with actin stress fibers in cells in interphase and with cortical actin at the cleavage furrow during mitosis (reviewed by Saarikangas and Barral, 2011; Mostowy and Cossart, 2012). Septins also colocalize with, and bind to subpopulations of microtubules, and regulate microtubule stability, post-translational modifications and microtubule-vesicle interactions (reviewed by Spiliotis, 2010). Septin 2 (SEPT2) directly interacts with MAP4, a ubiquitously expressed microtubule-associated protein (MAP) of the MAP2/TAU family, which positively regulates polymerization/stability of cytoplasmic microtubules. MAP4, which directly binds and bundles microtubules (reviewed by Holmfeldt et al., 2009), is thought to regulate septin-microtubule interactions (Kremer et al., 2005; Spiliotis et al., 2008) (reviewed by Spiliotis, 2010). Septins also associate with sub-domains of the plasma membrane by binding phosphatidylinositol-4,5-bisphosphate and, thereby, participate in mitosis, vesicular trafficking and morphogenesis of neurons (reviewed by Saarikangas and Barral, 2011; Mostowy and Cossart, 2012). Several septin binding partners have been identified including non-muscle myosin II and annillin in cytokinesis (Oegema et al., 2000; Kinoshita et al., 2002; Joo et al., 2007), and the sec6/sec8 subunits of the exocyst complex (Hsu et al., 1998). Finally, septins are also involved in the formation of cage-like structures around intracellular bacteria indicating that they also participate in host defense against pathogens (Mostowy et al., 2010).

Septins organize lateral membrane diffusion barriers between the ciliary compartment and the surrounding plasma membrane

in the sperm flagellum (Kissel et al., 2005; Ihara et al., 2005), primary cilium (Hu et al., 2010) and motile cilia (Kim et al., 2010b) (reviewed by Hu and Nelson, 2011). Flagella and cilia are highly conserved structures in eukaryotes that are involved in sensing and transducing environmental cues (primary and motile cilia), the movement of fluids (motile cilia), and in cell motility (motile cilia and flagella). Cilia are composed of a bundle of microtubules, termed the axoneme, which is assembled from a modified centriole called the basal body. The assembly of the cilium (ciliogenesis) is a complex process that requires an evolutionarily conserved machinery termed intraflagellar transport (IFT). The IFT machinery is thought to select, import and transport ciliary components (IFT particles or trains) into and along the axoneme towards the assembling distal end of the axoneme; this kinesin-based anterograde transport is balanced by dynein-dependent retrograde transport of IFT trains back to the basal body (reviewed by Pedersen et Rosenbaum, 2008; Ishikawa and Marshall, 2011).

The primary cilium, a specific subtype of sensory non-motile cilia, is present in most cells in vertebrates during development and in the adult depending on the cell type. The primary cilium controls key signaling pathways during development and tissue homeostasis. This was clearly demonstrated by the identification of genes mutated in complex genetic diseases associated with polycystic kidney, retinal degeneration, polydactyly and obesity that are generally referred to as ciliopathies (reviewed by Hildebrandt et al., 2011). Many, if not all the proteins encoded by these genes are localized near the basal body, the transition zone or within the primary cilium. The transition zone includes the region where the basal body is docked onto the cellular membrane, and extends distally to link microtubule doublets to the ciliary membrane by Y-shaped molecular links (Gilula and Satir, 1972). The transition zone may form a molecular filter between the ciliary compartment and the cytoplasm similar to the role of the nuclear pore complex (reviewed by Hu and Nelson, 2011; Ishikawa and Marshall, 2011). Septins form a ring-shaped structure at the base of cilia (Hu et al., 2010; Kim et al., 2010b; Chih et al., 2012). This localization is in agreement with a putative septin-based diffusion barrier at the transition zone. In addition, retention at the plasma membrane has been proposed to explain exclusion of membrane proteins from the cilium (Francis et al., 2011). SEPT2 is also required for ciliogenesis (Hu et al., 2010; Kim et al., 2010b; Chih et al., 2012), thereby linking septins to ciliary function and morphogenesis.

To further characterize these new functions of septins in the primary cilium, we investigated the distribution of septins in human telomerase-immortalized retinal pigment epithelial [hTERT-RPE-1 (RPE1)] cells, one of the most widely used models to study ciliogenesis. We found that in RPE1 cells SEPT2 forms a 1:1:1 complex with SEPT7 and SEPT9, that this complex localizes along the entire length of the axoneme, and that it positively controls ciliogenesis and the length of cilia. MAP4 is also localized to the axoneme, and negatively regulates ciliary length and therefore appears to antagonize the function of septins in the cilium.

Results

SEPT2, SEPT7, SEPT9 form a complex and localize to the primary cilium

SEPT2 forms a diffusion barrier at the base of the primary cilium in murine kidney (IMCD3) cells and fibroblasts (Hu et al., 2010; Chih et al., 2012; Garcia-Gonzalo et al., 2011). In IMCD3 cells, SEPT2 is also distributed along the axoneme in a minor proportion of the cells (Hu et al., 2010). To further characterize septins at the primary cilium, we analyzed the distribution and function of septins in RPE1 cells, a widely used *in vitro* cell model for ciliogenesis.

RPE1 cells were grown to confluency and then transferred to low serum medium for 24 hours to induce ciliogenesis. Under these conditions, 80% of the cells formed a cilium (Molla-Herman et al., 2010), which was identified as a 3–4 μm rod that stained for acetylated tubulin (AcTub). To identify septin complexes in these cells, lysates from ciliated cells expressing SEPT2–S-tag–GFP were sequentially precipitated with GFP antibodies followed by S-beads, and analyzed by SDS-PAGE using silver staining (Fig. 1A) and western blotting (Fig. 1B). The results show that SEPT2 is present in an apparently equimolar complex of SEPT2/SEPT7/SEPT9 in ciliated RPE1 cells.

The localization of the SEPT2/SEPT7/SEPT9 complex was then investigated in ciliated RPE1 cells. In ciliated (and in non-ciliated RPE1 cells) septins were organized as cytoplasmic fibers (Fig. 1C) that colocalized with actin filaments throughout the cell (see below). In addition, in the great majority of ciliated cells (see below), SEPT2, SEPT7 and SEPT9 colocalized with AcTub (Fig. 1C), indicating their presence in the primary cilium. Similar results were obtained in ARPE19 cells, another human RPE cell lines (supplementary material Fig. S1). SEPT9_v1 fused with Tomato (SEPT9–tomato) and transiently expressed in RPE1 cells also colocalized with AcTub in the primary cilium in fixed cells (data not shown). In live cells, SEPT9–tomato also colocalized with the somatostatin receptor type 3 (SSTR3–GFP; see below), a ciliary membrane marker (Händel et al., 1999; Berbari et al., 2008; Hu et al., 2010), showing that its localization to the primary cilium was not a fixation artifact. Altogether, these results indicate that a specific complex of septins (SEPT2/SEPT7/SEPT9) localized to the primary cilium in RPE cells.

Septins are present at the axoneme of cilia *in situ*

The presence of septins at the axoneme of cilia *in situ* was then further analyzed by immunohistochemistry of various human tissues. As shown in Fig. 2A, SEPT2 was abundant in the photoreceptor layer of the human retina in both the outer nuclear layer and the outer plexiform layer, which contains the presynaptic terminals of photoreceptor cells. SEPT2 colocalized with centrin3 a marker of the connecting cilium, the basal body and the adjacent daughter centriole of photoreceptor cells (Fig. 2A, bottom part). SEPT2 was also present in spots surrounding the daughter centriole but the significance of this staining remains to be determined. Moreover, we found staining of SEPT2 in the photoreceptor outer segments (Fig. 2A), which represent ciliary modifications. In addition, to SEPT2 in the retina, SEPT9 colocalized with AcTub at primary cilia of kidney tubule epithelial cells (Fig. 2B) and cilia of bronchus multiciliated epithelial cells (Fig. 2C); similar results were obtained for SEPT7 (data not shown). Thus, septins are components of the axoneme of primary cilia in RPE cell lines *in vitro* and in cilia of different tissues *in vivo*.

Septins accumulate in the axoneme of long mature primary cilia in RPE1 cells

Because localization of septins within axonemes was not detected in all ciliated RPE1 cells (see below) and only in a minor

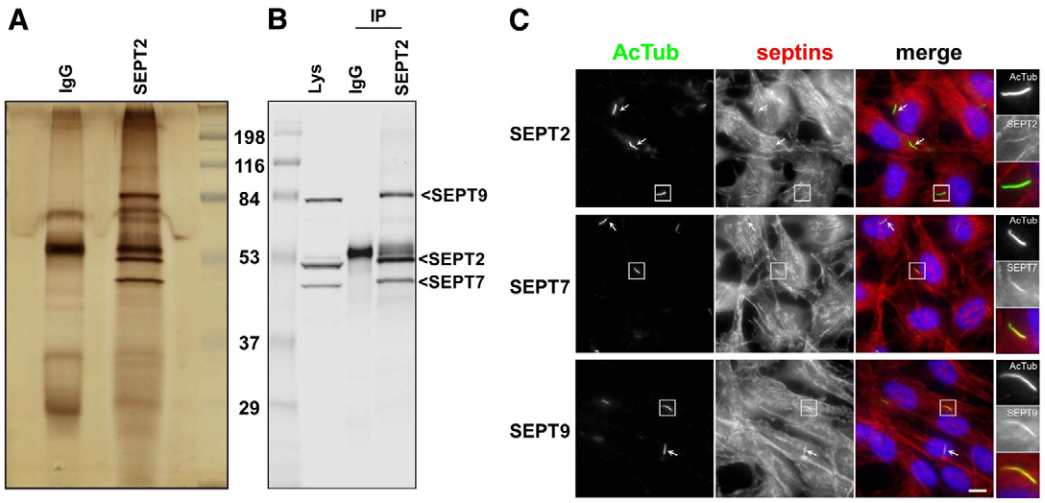

Fig. 1. A SEPT2/SEPT7/SEPT9 complex at the primary cilium of RPE1 cells. (**A**,**B**) RPE1 cells expressing SEPT2–S-tag–GFP were extracted and proteins immunoprecipitated either with control antibody (IgG) or GFP followed by S-beads (IP), and proteins separated by SDS-PAGE and processed for silver staining (A), or western blotting with a mixture of antibodies to SEPT9_v1, SEPT7 and SEPT2 (B). (**C**) RPE1 cells, grown on coverslips and serum-starved for 24 hours, were processed for immunofluorescence using anti-acetylated tubulin antibody to stain cilia (AcTub, green), antibodies against SEPT2, SEPT7 or SEPT9 (red), and DAPI (blue) to stain the nuclei. Panels on the right are enlarged views of representative cilia (boxed in the main images). White arrows indicate other cilia in the same field. Scale bar: 5 µm.

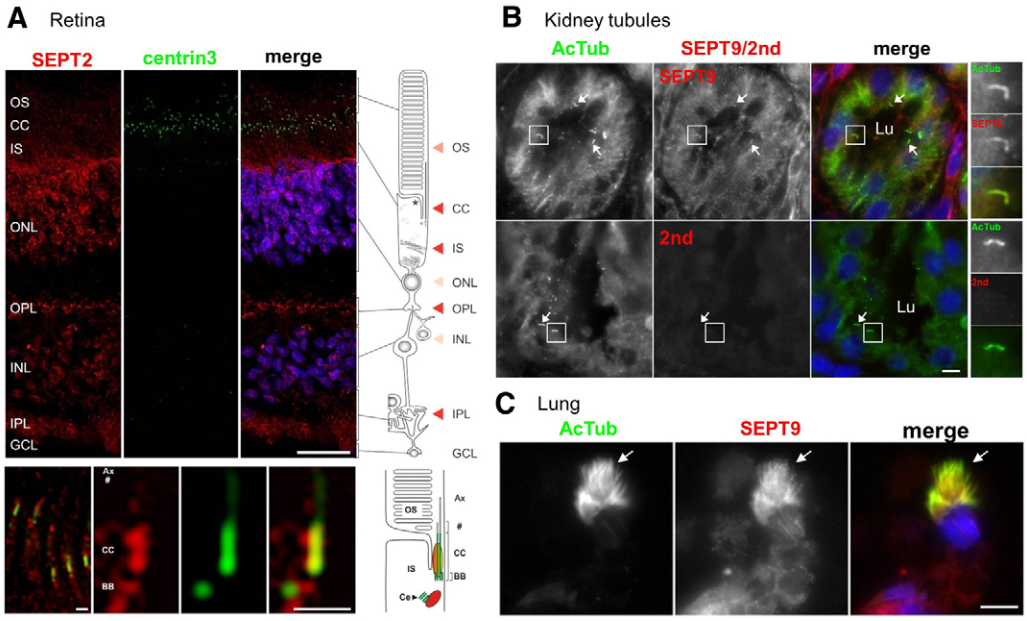

Fig. 2. Septins localize to the axoneme of cilia *in vivo*. (**A**) Indirect immunofluorescence triple staining of SEPT2 (red), centrin isoform 3 (green), which was used as marker for the connecting cilium (CC), basal body and the adjacent centriole (Ce), and nuclei were stained with DAPI (blue). In the human retina, SEPT2 is localized in the outer segment (OS), the inner segment (IS) and the synaptic compartments of the outer (OPL) and inner (IPL) plexiform layer. Additional weak staining was detected in the nuclei of the outer (ONL) and inner nuclear layer (INL). The bottom panel shows high magnification indirect immunofluorescence of SEPT2 (red) and centrin3 (green) in longitudinal cryosections through human photoreceptor cells. The high magnification reveals SEPT2 localization as a fibrous pattern in the inner and outer segment. Merged images reveals partial colocalization of SEPT2 with centrin3 at the centriole, the basal body (BB) and along the connecting cilium. Scale bars: top, 25 µm; bottom, 1 µm. (**B**) Tissue sections from adult human kidney were stained with antibodies against AcTub (red) and either SEPT9 (green) or with secondary anti-rabbit antibodies only (2nd; green). Nuclei were stained with DAPI (blue). Representative tubule lumens are indicated (Lu). Higher magnifications of representative cilia are shown on the right, and other cilia are identified with white arrows. Scale bar: 5 µm. (**C**) Tissue sections from the lung of a 33-week fetus were stained with antibodies against AcTub (red) and SEPT9 (green). White arrows point to a representative ciliary tuft. Scale bar: 5 µm.

proportion of the primary cilia in IMCD3 epithelial cells (Hu et al., 2010), we investigated whether the incorporation of septins into the primary cilium was dependent on state of cilium maturation.

The expression of some ciliary proteins is upregulated during ciliogenesis owing to a specific transcription program controlled by the RFX transcription factors family (reviewed by Thomas et al., 2010). Therefore, we examined the expression level of SEPT2/7/9 during ciliogenesis in RPE1 cells grown in the presence of serum, or in low serum for 24 or 48 hours. As shown in Fig. 3A, expression of SEPT2/SEPT7/SEPT9 was not significantly modified upon ciliogenesis, a result in agreement with the observations that the overall cytoplasmic network of septins appears similar in ciliated and non-ciliated cells and that septins at the cilium probably represents a very minor pool of the total cellular septins.

Next, we examined septin localization in the primary cilium at different times after withdrawal of serum and, thereby, different lengths of cilia. RPE1 cells were grown in a low serum concentration for 6 hours (~1 μm primary cilium; Fig. 3B) and 48 hours (~4 μm primary cilium; Fig. 3C), fixed and stained for AcTub and SEPT9 (Fig. 3). Although SEPT9 was absent from the axoneme of short 'young' cilia (6 hours, Fig. 3B), long 'mature' primary cilia (48 hours) had strong septin staining (Fig. 2C; >80% of septin-positive cilia, see below). Similar results were obtained for SEPT7 (supplementary material Fig. S2A). Therefore, septins accumulate in long, mature primary cilia. This observation was confirmed in live RPE1 cells that transiently co-expressed SEPT9–tomato and SSTR3–GFP. Forty-eight hours after serum starvation, a mixture of short and long primary cilia were detected in the cell population (Fig. 2D,E). Similar to endogenous SEPT9, SEPT9–tomato was absent or only stained the base of short primary cilia (Fig. 3D), whereas it decorated the length of long primary cilia (Fig. 3E). Note, however, that SEPT9–tomato (Fig. 3E, arrowheads) did not appear to localize at the tip of primary cilia. Similar observations were made using a SEPT2–GFP fusion (data not shown). These results indicate that septins accumulate in mature primary cilia by a process that probably depends on their gradual accumulation during ciliogenesis.

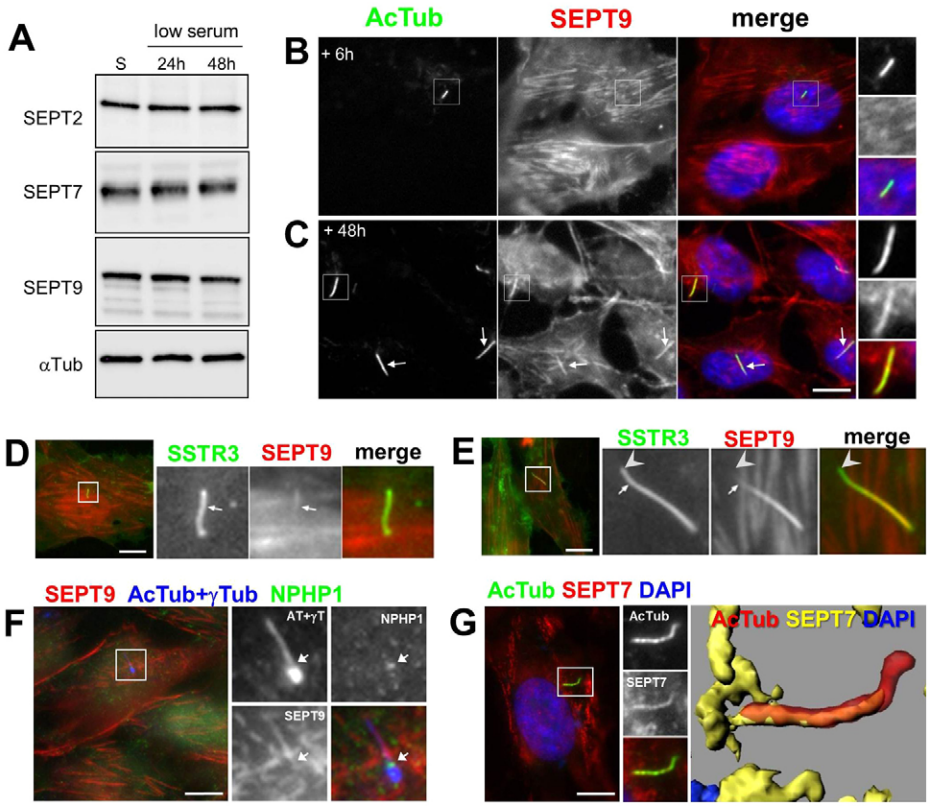

Fig. 3. Septins localize to the axoneme of long mature cilia in RPE1 cells. (**A**) RPE1 cells maintained in the presence of serum (S) or grown in low serum for 24 (24 h) or 48 (48 h) hours were lysed and expression of SEPT2, SEPT7 and SEPT9 was analyzed by western blotting with the indicated antibodies, expression of γ-tubulin was also analyzed in the same conditions as a control. (**B**,**C**) RPE1 cells, serum-starved for 6 (B) or 48 hours (C), were processed for immunofluorescence using antibodies against acetylated tubulin (AcTub; green) and anti-SEPT9 (red). Similar results were obtained using an anti-SEPT7 antibody (supplementary material Fig. S2). Panels on the right are enlarged views of representative cilia (boxed in the main images). (**D**,**E**) RPE1 cells were transiently transfected with plasmids encoding SSTR3–GFP (green) and SEPT9–tomato (red) fusions, serum-starved for 48 hours and directly analyzed by epifluorescence microscopy. Representative short (D) and long (E) cilia are shown. Panels on the right are enlarged views of each cilium (white boxes). Arrows and arrowheads indicate the distal end of SEPT9 and SSTR3 stainings, respectively. (**F**) RPE1 cells, serum-starved for 24 hours were processed for immunofluorescence using a mix of mouse monoclonal antibodies against acetylated-tubulin and γ-tubulin (AcTub+γTub; blue), a goat polyclonal against NPHP1 (green) and a rabbit polyclonal against SEPT7 (red). Panels on the right are enlarged views of a representative cilium (boxed in the main images) where the white arrows indicate NPHP1 staining. (**G**) RPE1 cells starved for 48 hours were stained for acetylated-tubulin (AcTub, green) and SEPT7 (red). Stacks of images were deconvoluted (left panels) and 3D reconstruction images (right) showed that SEPT7 staining overlaps with AcTub. Scale bars: 5 μm.

Septins colocalized with AcTub within the axoneme of long mature cilia (Figs 1, 3). To examine whether septins were present at other regions of the primary cilium, we compared the distribution of SEPT9 to that of markers of the axoneme (AcTub), basal body (γ-tubulin) and transition zone (NPHP1). Whereas SEPT9 colocalized with AcTub, we detected little or no colocalization with any of the other markers (Fig. 3F). Three-dimensional reconstruction of deconvoluted images clearly showed an almost complete overlap between AcTub and SEPT7 (Fig. 3G) indicating that septins accumulate all along the axoneme of long, mature cilia in RPE1 cells.

Localization of septins to the primary cilium of RPE-1 cells is independent of actin polymerization

Septins colocalize with actin cables throughout the cytoplasm in almost all non-dividing cell types, and with stable cytoplasmic microtubules in Madin–Darby canine kidney (MDCK) epithelial cells and other cell types (reviewed by Spiliotis, 2010). We compared the distribution of septins, the actin cytoskeleton and microtubules in RPE1 cells; SEPT2, SEPT7 and SEPT9 had identical distributions (see Fig. 1), so we show a detailed analysis of SEPT7 (Fig. 4), although similar observations were made with SEPT9 (supplementary material Fig. S3, and data not shown). In non-ciliated interphase RPE1 cells, SEPT7 colocalized with actin filaments (stress fibers) but not with cytoplasmic AcTub-positive microtubules (supplementary material Fig. S2B). During mitosis, SEPT7 colocalized with filamentous actin at the cell cortex and at the cleavage furrow, but not with microtubules at the mitotic spindle or midbody (supplementary material Fig. S2C, arrows). In ciliated RPE1 cells, SEPT7 mainly localized with actin filaments in the cytoplasm (Fig. 4A,a), but not with the general microtubule population (Fig. 4A,b) except within the cilium (Fig. 4Ac). Therefore, it appears that in RPE1 cells, septins mainly colocalize with actin filaments in the cytoplasm, and with microtubules in the cilium.

The polymerization state or contractility of the actin-based cytoskeleton were shown recently to be involved in ciliogenesis (Kim et al., 2010a; Bershteyn et al., 2010; Pitaval et al., 2010). Because the distribution of septins on cytoplasmic filaments depends on actin polymerization (Kinoshita et al., 2002), we tested the role of actin polymerization on the localization of septins to the primary cilium. Disruption of actin filaments using cytochalasin D resulted in a dramatic change in the distribution of cytoplasmic septin filaments into ring-like structures that colocalized with actin aggregates (Fig. 4B), as previously described (Kinoshita et al., 2002). However, addition of cytochalasin D did not affect SEPT7 localization in the primary cilium (Fig. 4B). When non-muscle myosin II was inhibited by blebbistatin, cytoplasmic septins filaments were shorter and their staining at the cortex increased, whereas staining of septins in the primary cilium was again unaffected (supplementary material Fig. S3). Thus, the actin-based cytoskeleton does not appear to be involved directly in the steady state localization of septins at the cilium.

Primary cilium-associated septins are stable, and non-dynamic

Since the axoneme forms the rails for the IFT trains, we examined whether or not axonemal septins are involved in IFT-like movements. RPE1 cells co-expressing SSTR3–GFP and SEPT9–tomato were imaged by live-cell fluorescence microscopy (Fig. 5A). SEPT9–tomato colocalized with SSTR3–GFP in cilia in live cells and was uniformly distributed along the length of cilia (Fig. 5A, arrows) as observed in fixed cells (Figs 1, 2). SEPT2–GFP also localized along the length of the cilium (Fig. 5B–D, and data not shown). These distributions are different from the more punctate organization of IFT particles that move within the cilium and accumulate at the basal body and/or the distal tip (review by Pedersen and Rosenbaum, 2008; Ishikawa et Marshall, 2011).

To further explore the organization of septins in the primary cilium, we investigated their dynamics using fluorescence recovery after photobleaching (FRAP). We first tested whether septins within the axoneme exchanged with the cytoplasmic pool. RPE1 cells co-expressing pericentrin–RFP to identify the basal body, and SEPT2–GFP were imaged by live-cell fluorescence microscopy (Fig. 5B–D). Following photobleaching (Fig. 5B; white boxes), the recovery rate of primary-cilium-associated SEPT2–GFP fluorescence (arrows) was compared to that of cytoplasmic septin filaments (arrowheads). Whereas fluorescence

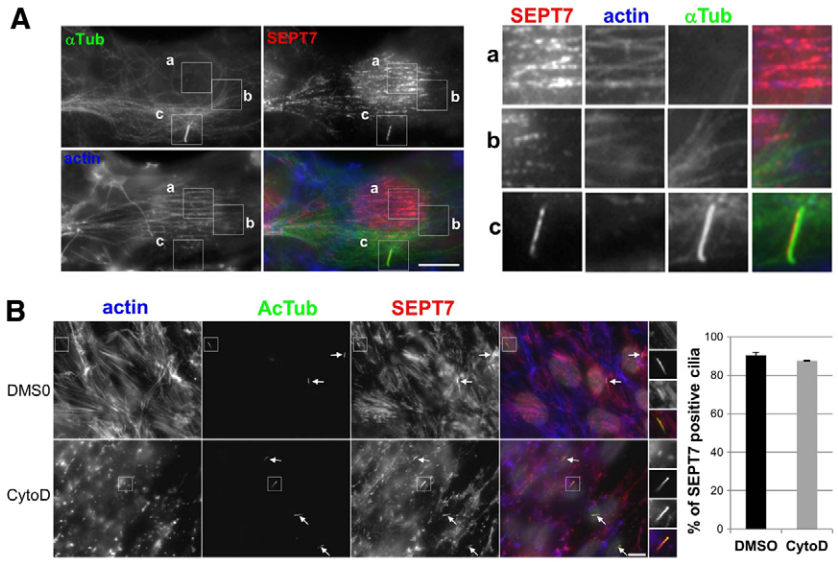

Fig. 4. Localization of septins to the primary cilium does not depend on actin polymerization. (**A**) RPE1 cells were serum starved for 24 hours and then fixed and stained for immunofluorescence using antibodies against SEPT7 (red), α-tubulin (α-Tub; green), and fluorescent phalloidin to stain actin filaments (blue). Panels on the right are enlarged views of representative regions of the same cell (boxed in the main images) including stress fibers (a) microtubules (b) and the cilium (c). (**B**) RPE1 cells were serum-starved for 24 hours and then treated with 5 μM cytochalasin D (CytoD) or, as a control, with the same final concentration of DMSO, for 30 minutes at 37℃, then fixed and analyzed by immunofluorescence using antibodies against SEPT7 (red), acetylated tubulin (AcTub; green) and fluorescent phalloidin (actin; blue). Panels on the right are enlarged views of representative cilia (boxed in the main images). White arrows point to cilia in the same field. Scale bars: 5 μm. (Far right) Results were quantified (i.e. proportion of SEPT7-positive cilia) from three independent experiments (n=40 cilia per experiments).

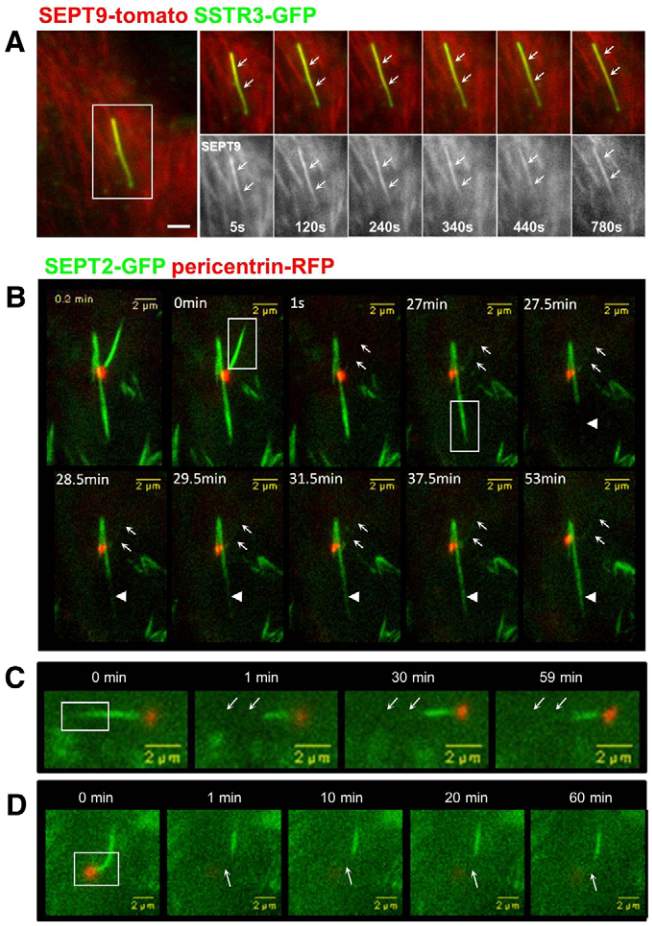

Fig. 5. Septins form a stable-non dynamic pool at the primary cilium. (**A**) RPE1 cells were transiently transfected with plasmids coding for SSTR3–GFP (green) and SEPT9–tomato (red) fusions, then serum-starved for 48 hours and analyzed by live-cell epifluorescence microscopy. An example of the behavior of SEPT9 in a long cilium is shown (one image every 5 seconds; from left to right). White arrows indicate the position of the cilium. (**B–D**) RPE1 cells were transiently transfected with plasmids coding for SEPT2–GFP (green) and pericentrin–RFP (red) fusions, then serum-starved for 48 hours and analyzed by live-cell confocal microscopy. The dynamic of SEPT2 at the cilium (B–D) or in cytoplasmic filaments (B) was analyzed by FRAP. Regions (boxed in the main images) including the whole cilium (0 min) or a cytoplasmic SEPT2 filament (27 min; B), the distal part (C) or the proximal part (D) of the cilium were photobleached and recovery of the GFP fluorescence was analyzed for the indicated period. White arrows point to the position of the cilia before photobleaching. Scale bars: 2 µm.

of the cytoplasmic pool of septins recovered slowly over 4 minutes, SEPT2–GFP fluorescence in the primary cilium did not, even when the recovery time was extended to more than 50 minutes. Similar results were obtained using the SEPT9–tomato fusion (supplementary material Fig. S5). These data indicate that in addition to being associated with distinct structures, cytoplasmic and cilium-associated septins represent different dynamic pools that do not appear to exchange with each other.

To test whether septins are dynamic within primary cilium, SEPT2–GFP was photobleached in the distal (Fig. 5C) or proximal (Fig. 5D) domain of the primary cilium. The photobleached regions of SEPT2–GFP did not appear to recover fluorescence. Since the fluorescence of SEPT2–GFP in short, immature primary cilia was very weak, we were unable to analyze septin dynamics in those cilia. Nevertheless, the results in mature primary cilia indicate that septins are not dynamic and may be a structural component of the axoneme.

Septins are required for ciliogenesis and control cilium length in RPE1 cells

To test the functions of septins during ciliogenesis in RPE1 cells, we use the septin targeting drug Forchlorfenuron which induces the assembly of large septins structures and perturbs septin dynamics without affecting either actin or tubulin polymerization (Hu et al., 2008). While treatment of RPE1 cells with 50 µM Pestanal during ciliogenesis significantly reduced the percentage of ciliated cells (supplementary material Fig. S4A–C), a short treatment, of 4 hours, of ciliated cells only moderately affected ciliogenesis without perturbing the localization of septins to the axoneme (supplementary material Fig. S4D,E). Thus these results indicate that a dynamic septin network is necessary for ciliogenesis.

To more specifically investigate the role of each septin isoform in ciliogenesis we then used previously characterized siRNA sequences to knockdown expression of *SEPT7* (Kremer et al., 2005) or *SEPT9* (Mostowy et al., 2010), and a luciferase targeting sequence as a negative control. The efficiency and specificity of the knockdown was assessed by western blotting of septins, using the ubiquitously expressed clathrin-adaptor complex AP-1 as a control (Fig. 6A). Two different SEPT7 siRNAs efficiently knocked down expression of *SEPT7*, and resulted in efficient downregulation of both SEPT2 and SEPT9. SEPT9 targeting siRNA also efficiently knocked down *SEPT9* expression, but had little effect on either *SEPT2* or *SEPT7* expression, as recently observed (see Discussion). These results were confirmed by immunofluorescence (Fig. 6B), and identify the key function of SEPT7 in the overall stability of septin complexes (see Discussion).

The effect of septin depletion on ciliogenesis was investigated in RPE1 cells by immunofluorescence, and the proportion of ciliated cells and length of primary cilium were quantified based on AcTub staining, as described previously (Molla-Herman et al., 2010; Hu et al., 2010). The percentage of cells with cilia was normalized to controls (normalized ciliogenesis). Depletion of SEPT7 significantly inhibited ciliogenesis (49.9±14.2% of control; Fig. 6B,C) and the primary cilia that formed were shorter than those in control-siRNA-treated cells (1.81±0.61 µm versus 2.71±0.83 µm for control; Fig. 6D). Depletion of SEPT9 resulted in limited effects on the formation of cilia (92.9±10.7% of control; Fig. 6C). However, primary cilia in SEPT9-depleted cells were shorter than in control cells (1.69±0.52 µm versus 3.0±0.78 µm in controls; Fig. 6D), similar to SEPT7-siRNA-treated cells (Fig. 6D). These results indicate that the SEPT2/SEPT7/SEPT9 complex plays a role in ciliogenesis, and that SEPT9 is required to form long cilia.

The septin binding partner MAP4 localizes to the primary cilium and controls cilium length

To investigate the role of septins in controlling ciliogenesis and the length of the cilia, we focused on the possible role of MAP4 because it has been shown to regulate microtubule–septin interactions and function (Kremer et al., 2005; Spiliotis et al., 2008). MAP4 is a ubiquitously expressed MAP of the

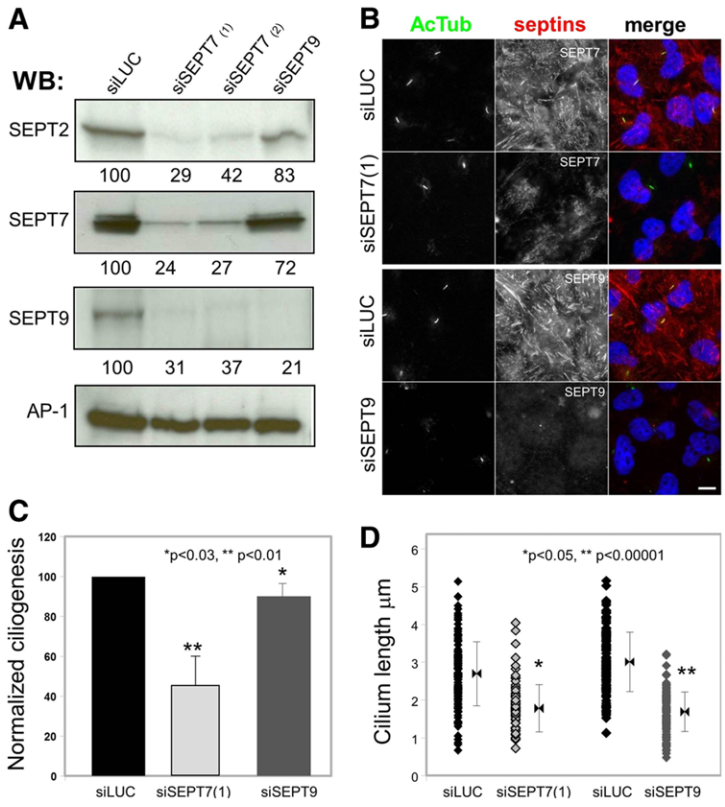

Fig. 6. Septins are required for ciliogenesis, and control cilium length. (**A**) RPE1 cells were treated with a control luciferase-targeting siRNA (siLUC), two different SEPT7-specific siRNA [siSEPT7(1) and siSEPT7(2)] or a SEPT9-specific siRNA (siSEPT9) were analyzed by western blotting using antibodies against the indicated septins and the γ-adaptin subunit of the AP-1 complex as a control. A quantification of the signal is shown below each panel. (**B**) RPE1 cells treated with siSEPT7(1), SEPT9 or luciferase targeting siRNA were analyzed by immunofluorescence using antibodies against SEPT7 or SEPT9 (red) and acetylated-tubulin (AcTub; green). (**C**) The ability of siRNA-treated cells to form primary cilia was analyzed by immunofluorescence from images obtained as in B. Results were quantified (i.e. cells with a single rod-like AcTub-positive structure), normalized to control cells in each experiments and expressed as normalized ciliogenesis. Statistical analysis was performed with the Student's *t*-test. (**D**) The length of cilia in siRNA-treated cells was measured ($n=50$) and the length distribution is shown. Results are from three independent experiments. Statistical analysis was performed with the Fischer test. Scale bar: 5 µm.

MAP2/TAU family that increases the assembly and stability of cytoplasmic microtubules (reviewed by Holmfeldt et al., 2009). However, neither the localization of MAP4 in primary cilia nor its functions in ciliogenesis have been examined.

Endogenous MAP4 colocalized with AcTub in the primary cilia of RPE1 cells fixed in either methanol (Fig. 7A), which allowed co-staining of MAP4 and cytoplasmic microtubules, or paraformaldehyde (Fig. 7B). Similar results were obtained in human primary foreskin fibroblasts (supplementary material Fig. S6). We also examined the localization of a GFP fusion of a truncation mutant of *MAP4*, which encodes amino acid (aa) 800–1152 (GFP–MAP4m) and includes most of the proline-rich domain and the affinity domain (termed PRD and AD, respectively). This mutant has been used in functional studies where it was shown to bind and stabilize microtubules (Nguyen et al., 1997; Perez et al., 1999). GFP–MAP4m colocalized with AcTub in the primary cilia of all ciliated GFP–MAP4m-expressing cells (Fig. 7C). This result confirms observations made with the MAP4 antibody, and indicates that the C-terminal microtubule-binding domain of MAP4 (PRD and AD) contains a primary cilium-targeting domain. Additional localization analysis using myc-tagged deletion mutants of MAP4 confirmed that the PRD (aa 654–895) contains the primary cilium-targeting domain, therefore, indicating that this motif is present between aa 800 and 895 of MAP4 (supplementary material Fig. S7).

Localization of MAP4 at cilia *in vivo* was also investigated in the human retina, in a similar manner to that for SEPT2 (Fig. 2). Analyses of parallel sections by immunofluorescence double labeling of anti-MAP4 and centrin3 in human retinal sections also revealed colocalization of MAP4 and centrin3 (Fig. 7D) at the connecting cilium and the basal body. MAP4 was also present in the outer segment with a linear distribution, indicating its localization along the axoneme (arrows). Together with results presented in Fig. 2A, these results show the expression of SEPT2 and MAP4 in the same subciliary compartments of retinal photoreceptor cells.

The role of MAP4 in ciliogenesis was investigated using an siRNA-based approach in RPE1 cells. Two previously characterized MAP4-targeting siRNA (Holmfeldt et al., 2007) were used in RPE1 cells, and their effects on MAP4 expression, ciliogenesis and cilium length were analyzed by immunofluorescence as described above for septins. The two siRNAs efficiently knocked down *MAP4* expression with similar efficiencies (Fig. 8A). In general, ciliogenesis was only moderately affected in MAP4-depleted cells compared to control siRNA-treated cells {83.1±7.9% [siMAP4(1)] and 92.9±11.3% [siMAP4(2)] of control; Fig. 8B and C} although the primary cilia that formed in MAP4-depleted cells were ~1.1 µm longer than in control cells {4.27 [siMAP4(1)] and 4.29 [MAP4(2)] versus 3.15 µm for control, Fig. 8D}. Importantly, depletion of MAP4 did not affect the expression of septins (supplementary material Fig. S8) (see also Kremer et al., 2005). These results show that MAP4 is a component of the primary cilium, and that its presence may be required to limit the growth of the axoneme.

MAP4 competes with septins at the axoneme

It was described previously that MAP4 negatively regulates interaction of septins with microtubules (Kremer et al., 2005; Spiliotis et al., 2008). In addition, MAP4 is present at the axoneme of human primary fibroblasts (supplementary material Fig. S6) where SEPT2/7/9 could not be detected (data not shown), indicating that localization of MAP4 at cilia does not depend on septins. We next investigated the role of MAP4 in the localization of septins at the axoneme.

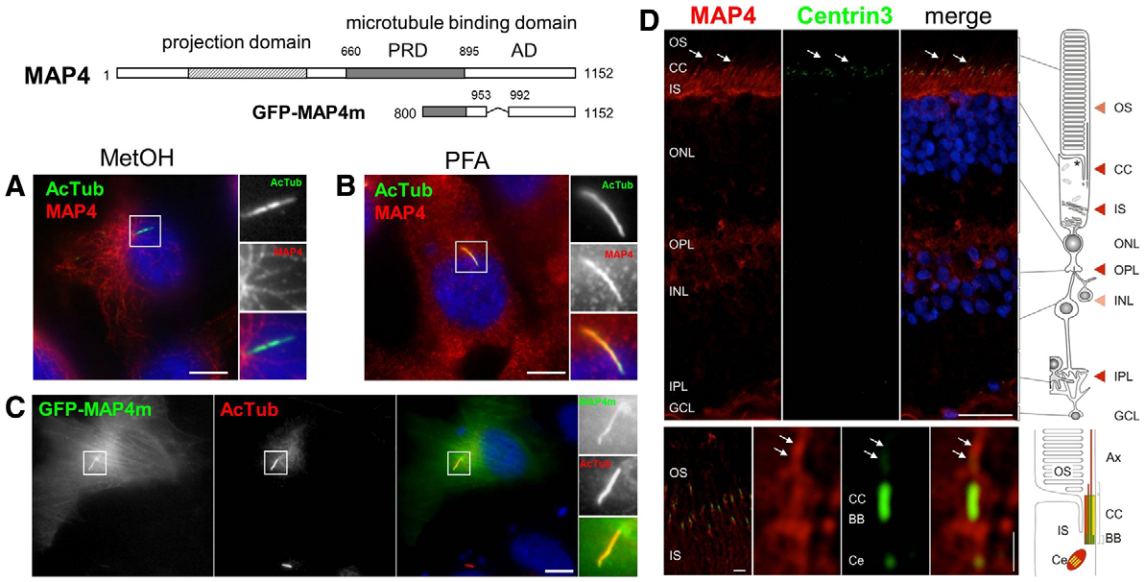

Fig. 7. MAP4 localizes to the primary cilium in RPE1 cells. Schematic representation of MAP4 showing its functional domains and the region encoded by the GFP-MAP4m fusion. PRD, proline-rich domain; AD, affinity domain. (**A**,**B**) RPE1 cells were grown on coverslips, serum-starved for 48 hours and then fixed with methanol (MetOH; A) or paraformaldehyde (PFA; B) then processed for immunofluorescence using anti-acetylated tubulin (AcTub, green) and anti-MAP4 (red) antibodies, and DAPI (blue) to stain nuclei. (**C**) RPE1 cells were transiently transfected with the GFP-MAP4m encoding plasmid, fixed and processed for immunofluorescence using an antibody against acetylated-tubulin (red) and DAPI (blue) to stain nuclei. Panels on the right are enlarged views of representative cilia (boxed in the main images). Scale bars: 5 µm (A–C). (**D**) Indirect immunofluorescence staining of MAP4 (red), centrin3 (green), used as marker for the connecting cilium (CC), basal body and the adjacent centriole (Ce), and the nuclei were stained with DAPI (blue). In the human retina MAP4 is localized in the outer segment (OS) and in the inner segment (IS) of the outer plexiform layer (OPL). Bottom panel shows high magnification indirect immunofluorescence of MAP4 (red) and centrin3 (green) in longitudinal cryosections through human photoreceptor cells. Merged images reveal partial colocalization of MAP4 with centrin3 at the centriole, the basal body (BB) and along the connecting cilium and axoneme (white arrows). Scale bars: top, 25 µm; bottom, 1 µm.

The localization of septins at cilia was analyzed in RPE1 cells treated with siMAP4(1), in conditions in which most of the cells (>90%) showed effective knockdown of *MAP4* expression (i.e. similarly to conditions shown in Fig. 8). The proportion of cilia (AcTub) that stained for SEPT7 was quantified and compared to control siLUC-treated cells. As shown in Fig. 9A, SEPT7

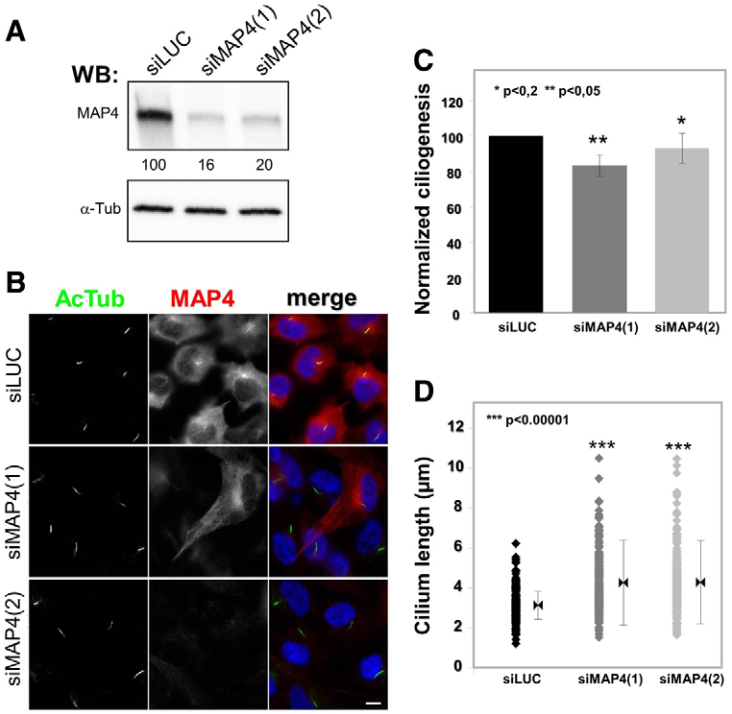

Fig. 8. MAP4 negatively regulates cilium length. (**A–D**) RPE1 cells were treated with two different MAP4-specific siRNAs [siMAP4(1) and siMAP4(2)] or luciferase targeting siRNA (siLUC) as a control. Expression of MAP4 was analyzed by western blotting (A), using antibodies against MAP4 and α-tubulin (α-tub) as a control, and by immunofluorescence (B), using antibodies against acetylated tubulin (AcTub; green) and MAP4 (red). (C) The ability of siRNA-treated cells to form cilia was analyzed by immunofluorescence from images obtained as in B. (C) The effects of MAP4 siRNA on ciliogenesis were quantified as in Fig. 6 and expressed as normalized ciliogenesis. Statistical analysis was performed with the Student's *t*-test. (D) The length of the cilia of siRNA-treated cells was measured as in Fig. 6 (n=50). Statistical analysis was performed with the Fischer test. Scale bar: 5 µm.

colocalized with AcTub in long cilia present in MAP4-depleted cells in a proportion similar to that for control cells (84.0 versus 71.6%, respectively). These data indicate that MAP4 is not required for the recruitment of septins to the axoneme of cilia.

Overexpression of MAP4 results in the mislocalization of septins from stable cytoplasmic microtubules (Kremer et al., 2005; Spiliotis et al., 2008). To test whether a similar competition could occur at the axoneme, which is also composed of stabilized microtubules, the distribution of septins at cilia was analyzed in ciliated cells expressing GFP–MAP4m (see Fig. 7) or SSTR3–GFP as a control. As expected, SEPT7 (Fig. 9B), as well as SEPT2 and SEPT9 (data not shown), did not colocalize with AcTub in most GFP–MAP4m-positive cilia (Fig. 9B, arrows). In contrast, septins were present in all SSTR3–GFP-positive control long cilia. These results support a general role of MAP4 as a negative regulator of septin functions at stabilized microtubules.

Discussion

The above results show that a SEPT2/SEPT7/SEPT9 complex is present along the axoneme of the primary cilium of RPE cells where it appears to function as a positive regulator of ciliogenesis. We identified MAP4 along the axoneme of the primary cilium where it appears to function as a negative regulator of ciliary length. Therefore, MAP4 and septins appear to function antagonistically to control ciliogenesis and the length of the primary cilium.

Our proteomic analysis revealed a complex of SEPT2/SEPT7/SEPT9 in a ~1:1:1 stoichiometry in RPE1 cells, and all three of these septin isoforms had overlapping distributions in the cytoplasm of RPE1 cells, and prominently at the axoneme of the primary cilium of quiescent RPE1 cells (Figs 1, 3, 4). Similar overlapping distributions of SEPT2/SEPT7/SEPT9 were observed in ARPE19 cells, another RPE cell line (supplementary material Fig. S1). A previous study showed that SEPT2 localized to the base the primary cilium of quiescent IMCD3 kidney cells (Hu et al., 2010), but that it also formed puncta along the axoneme in a minority of these cells (Hu et al., 2010). Interestingly, a recent proteomic study revealed that SEPT2, SEPT7 and SEPT9 are present in IMCD3 cilia (Ishikawa et al., 2012).

Several other proteomic studies showed the presence of septins in the multiple primary cilia of choroid plexus epithelial cells (swine), in mouse photoreceptor connecting cilia and cilia of olfactory neurons from rat (Narita et al., 2012; Liu et al., 2007; Mayer et al., 2009). Finally our results show that septins are present within the axoneme of cilia in human tissues including connecting cilia of photoreceptors, primary cilia of kidney epithelial cells and motile cilia of the lung (Fig. 2). Taken together, these results demonstrate that septins are general components of cilia in vertebrates, but have distinct distributions, and possibly functions, in different tissues and cell types.

SEPT2, SEPT7 and SEPT9 were found at the axoneme of human RPE cells but not in human primary fibroblasts (data not shown). The molecular basis for different distributions of the same septins in the primary cilium of different cell types is unclear. However, it is interesting to note that SEPT7 and SEPT9 colocalized with AcTub in the primary cilium of the two RPE cell lines but were absent from cytoplasmic microtubules in RPE1 cells (Fig. 4; supplementary material Fig. S1); in contrast, SEPT7 and SEPT9 colocalized with AcTub microtubules in the cytoplasm, mitotic spindle and mid-body of ARPE19 cells (supplementary material Fig. S1B,C,E). These results indicate that the mechanisms controlling localization of septin to cytoplasmic microtubules and the axoneme are probably different, and that further studies are required to understand the underlying mechanisms.

We used FRAP and live-cell imaging to investigate whether SEPT2 and SEPT9 moved dynamically in the primary cilium. Our results showed that there was no exchange between the axonemal and cytoplasmic pools of septins nor movement of septins along the axoneme, indicating that septins are not a component of IFT (Fig. 5; supplementary material Fig. S5).

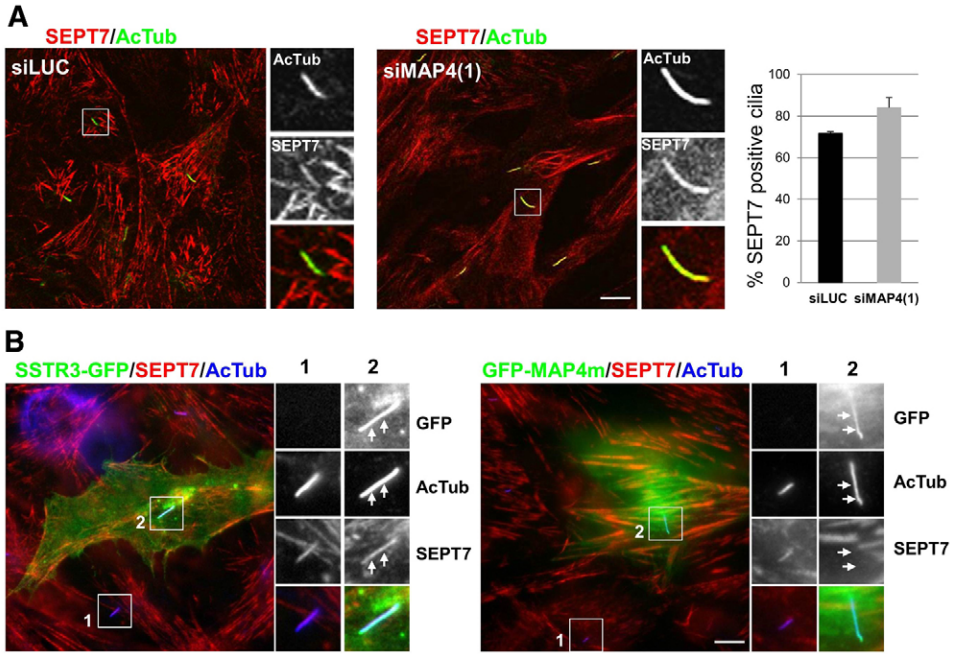

Fig. 9. MAP4 competes with septins at the axoneme. (**A**) RPE1 cells treated with siMAP4(1) or luciferase targeting siRNA (siLUC) as a control (as in Fig. 8) were stained with antibodies against acetylated tubulin (AcTub, green) and SEPT7 (red). Panels on the right are enlarged views of representative cilia (boxed in the main images). The proportion of SEPT7-positive cilia was quantified in both conditions from three independent experiments ($n=30$ in each experiment, $P>0.1$). (**B**) RPE1 cells were transiently transfected with SSTR3-GFP or GFP-MAP4m plasmids, fixed and processed for immunofluorescence with antibodies for SEPT7 (red) and acetylated tubulin (AcTub; blue), and the nuclei were stained with DAPI (blue). Panels on the right are enlarged views of representative cilia (boxed in the main images). White arrows indicate the position of cilia. Scale bars: 5 µm.

These data indicate differences in the dynamic properties of cytoplasmic and ciliary septins. They also support previous observations indicating that, with the exception of IFT components and signaling molecules, the ciliary membrane and axonemal compartments have low or very limited exchange with the rest of the cell. Finally, FRAP was also used to investigated the dynamics of the SSTR3–GFP, a well-characterized ciliary membrane protein, in cilia of RPE1 cells. Our results indicate that SSTR3–GFP dynamics are similar in the cilia of RPE-1 and IMCD3 cells (Hu et al., 2010; Chih et al., 2012), with low if any recovery after photobleaching of the whole cilium (supplementary material Fig. S9A,A′). In addition, SSTR3–GFP can also diffuse within the ciliary membrane (supplementary material Fig. S9B,B′). Thus the presence of septins along the axoneme does not appear to prevent the movement of membrane proteins in the ciliary membrane.

To investigate the functions of septins in RPE1 cilia, we depleted septins using a siRNA-based approach. As previously described (Kremer et al., 2005; Tooley et al., 2009; Sellin et al., 2011), efficient knockdown of *SEPT7* resulted in the concomitant loss of the other two members of the complex, SEPT2 and SEPT9. Under these conditions, ciliogenesis was inhibited in ~50% of cells, and the primary cilia in the remaining ~50% of cells were significantly shorter than in the control. SiRNA-targeted depletion of SEPT9 affected SEPT9 levels but not those of SEPT2 or SEPT7 (see also Tooley et al., 2009; Estey et al., 2010; Sellin et al., 2011), and resulted in little or no effect on ciliogenesis, although the primary cilia were shorter. These results indicate that the SEPT2/SEPT7/SEPT9 complex is required for ciliogenesis in RPE1 cells, as shown previously for SEPT2 in IMCD3 cells (Hu et al., 2010; Chih et al., 2012), and that SEPT9 is specifically required for the proper elongation of cilia. The importance of SEPT9 is in agreement with recent data showing that SEPT9 plays a crucial role in the elongation of septin filaments because of its terminal position within septins oligomers (Kim et al., 2011). In conclusion, the assembly of septin filaments plays a crucial role in the elongation of the primary cilium in RPE1 cells.

To further investigate the role of septins in the primary cilium, we examined MAP4, which regulates the functions of septins with cytoplasmic microtubules (Kremer et al., 2005; Spiliotis et al., 2008). MAP4 colocalized with AcTub along the axoneme of the primary cilium in RPE1 cells (Fig. 7), and in human primary fibroblasts (supplementary material Fig. S6). MAP4 is a well-established positive regulator of microtubule polymerization, and MAP4 depletion results in an increase in the pool of free tubulin, whereas overexpression of wild-type or mutant forms of MAP4 containing the microtubule-binding domain (including MAP4m) stabilizes microtubules and increases the proportion of polymerized tubulin (Nguyen et al., 1997; Nguyen et al., 1999; Holmfeldt et al., 2002; Holmfeldt et al., 2007). Interestingly, moderate treatment with nocodazole, which depolymerizes microtubules and increases the amount of free tubulin, results in longer cilia (Sharma et al., 2011), similar to what we observed when we depleted MAP4 in RPE1 cells (Fig. 8). As expected, treatment of MAP4-depleted RPE1 cells with moderate concentration of taxol, which stabilizes microtubules and decrease ciliary length (Sharma et al., 2011), reversed the effect of MAP4 depletion and resulted in shorter MAP4-depleted cilia (supplementary material Fig. S10). Part of the effect of MAP4 depletion on ciliary length could be interpreted as an indirect effect on the assembly of cytoplasmic microtubules and regulation of free tubulin pool. However, the presence of MAP4 within cilia (Fig. 7; supplementary material Fig. S6) indicates that MAP4 may also directly regulate the polymerization dynamics of axonemal microtubules.

Our results show that MAP4 is not required for the localization of septins to the cilium of RPE1 cells (Fig. 9A). Significantly, MAP4 was present in primary cilia in which the levels of SEPT2/7/9 were very low, such as human primary fibroblasts (supplementary material Fig. S6, and data not shown), indicating that MAP4 might compete with and/or displace septins from axonemal microtubules. Indeed, studies *in vitro* and *in vivo* have shown that MAP4 and septins compete for microtubule binding (Kremer et al., 2005; Spiliotis et al., 2008). Therefore, we speculate that in the primary cilium, MAP4 controls the accessibility of septins to the axoneme thereby negatively regulating ciliary elongation, an effect counteracted by septins in cell types such as RPE cells. In agreement with this hypothesis, septins were absent from cilia in cells expressing the MAP4m mutant (Fig. 9B).

The molecular basis for a cell-type-specific effect of MAP4 on the accessibility of septins to the axoneme remains to be determined. Regulation of MAP4 functions through alternative splicing (Chapin et al., 1995) and/or phosphorylation by MARK [MAP/microtubule affinity-regulating kinase (Drewes et al., 1997)] are two possibilities that should be investigated in the future. Interestingly, recent data obtained by G. Pereira's group (Kuhns et al., 2013) indicate that MARK4, a kinase known to phosphorylate MAP4 (Trinczek et al., 2004), is present at the basal body where it positively regulates ciliogenesis in a kinase-activity-dependent process.

In conclusion, our study reveals that septins and MAP4 probably play antagonistic roles in controlling axonemal microtubule organization and growth, similar to their functions with cytoplasmic microtubules. In addition, septins have different distributions within the primary cilium of different cell types indicating different functions and mechanisms of regulation.

Materials and Methods

Plasmids, antibodies and reagents

The Septin9_v1–tomato-encoding plasmid was described previously (Mostowy et al., 2010). The SSTR3–GFP-encoding plasmid was a generous gift from K. Mykytyn [Ohio State University (Berbari et al., 2008)]. The MAP4m–GFP-encoding plasmid was provided by F. Perez [Curie Institute (Perez et al., 1999)]. Mouse SEPT2 was subcloned from SEPT2-YFP to generate SEPT2–S-tag–GFP containing a TEV site between the S-tag and GFP, using Gateway subcloning (Invitrogen); RFP-pericentrin PACT domain (PeriCTRFP) was a gift from Sean Munro (MRC Laboratory of Molecular Biology, Cambridge, UK) (for details, see Hu et al., 2010). Mouse monoclonal antibodies against acetylated tubulin (clone 6-11B-1) and γ-tubulin (GTU-88) were from Sigma. Rabbit polyclonal antibody against MAP4 (sc-67152) and goat polyclonal against NPHP1 (sc-20204) were from Santa Cruz Biotechnologies. Rabbit polyclonal antibodies against SEPT2, SEPT7 and SEPT9 were described previously (Mostowy et al., 2009; Mostowy et al., 2010; Hu et al., 2010), or obtained from Sigma (SEPT7; HPA 029524). Monoclonal antibodies against mouse centrin3 were previously characterized and are frequently used as molecular markers of ciliary sub-compartments (Trojan et al., 2008). Alexa-Fluor-conjugated secondary antibodies (Alexa Fluor 488, Alexa Fluor 546 and Alexa Fluor 647) and Alexa-Fluor-546-conjugated phalloidin were purchased from Life Technologies (Molecular Probes). Cytochalasin D, blebbistatin, Forchlorfenuron, taxol and nocodazole were purchased from Sigma.

Cells

RPE1 cells, a human retinal pigment epithelial cell line that stably expresses human telomerase reverse transcriptase (hTERT-RPE1; Clontech Laboratories, Inc.), and ARPE19 cells, a spontaneously arising human retinal pigment epithelial cell line, were kind gifts from M. Bornens (Institut Curie, Paris, France) and Y. Courtois (Centre de Recherche des Cordeliers, Paris, France). Human inner foreskin fibroblasts (hFF) were a kind gift from Y. Ganor (Institut Cochin, Paris). RPE cells

were grown in Dulbecco's modified Eagle's medium (DMEM)-F12 (1:1) supplemented with 10% fetal bovine serum (FBS, Life Technologies) for RPE1 cells, and in DMEM supplemented with 10% fetal bovine serum (Life technologies) for hFF. To induce ciliogenesis, cells were grown to confluency on glass coverslips in basic cell culture conditions and then transferred into low serum (0.5% FBS) medium for an additional 24 or 48 hours, as described previously (Molla-Herman et al., 2010).

Transfections

Transfections of plasmids were performed following the recommended procedure for the FuGENE HD (Roche) transfection reagent. Subconfluent RPE1 cells grown on glass coverslips or on μ-slides (Ibidi) were transfected and immediately transferred to low serum conditions for 24 or 48 hours.

For knockdown experiments, RPE1 cells were treated with control siRNA [luciferase (*Luc*): 5′-GCCATTCTATCCTCTAGAGGATG-3′] or with siRNA targeting *SEPT7* [SEPT7(1): 5′-GTCGACATTAATCAACTCA-3′; SEPT7(2): 5′-GGCAGTATCCTTGGGGTGT-3′ (Kremer et al., 2005)], *SEPT9* [SEPT9: ID no. 18228 from Ambion (Mostowy et al., 2009; Mostowy et al., 2010)] or *MAP4* [MAP4(1): 5′-CTGGCCAGAAGATACCAAC-3′; MAP4(2): 5′-GATAGTCCC-AGCCAAGGAT-3′; (Holmfeldt et al., 2007)]. The siRNA duplexes, with the exception of SEPT9, were obtained from Eurogentec. Briefly, siRNA duplexes were transfected using Lipofectamine RNAiMAX transfection reagent (Life technologies) according to the manufacturer's instructions as described previously (Molla-Herman et al., 2010). RPE1 cells plated at 30% confluency (cells per well) were transfected on the first day with siRNA (50 nM) and then grown in basic conditions. Transfected cells were transferred to low serum media (0 or 0.5% serum) to induce ciliogenesis on the third or fourth day, as indicated, and then processed for immunofluorescence or biochemistry.

Immunofluorescence

Cells grown on glass coverslips were washed twice in PBS and fixed in methanol at −20℃ for 4 minutes, or in 4% paraformaldehyde for 20 minutes at 4℃. Fixed cells were incubated with primary antibodies in PBS containing 0.1% Triton X-100 (Sigma) and 1 mg/ml BSA (Sigma) for 45 minutes at room temperature. After two washes with PBS–BSA, cells were incubated for 30 minutes at room temperature in PBS–BSA containing secondary antibodies. After one wash with PBS–BSA and two washes in PBS, coverslips were mounted on microscope slides in a PBS–glycerol mix (50/50) using the SlowFade Light Antifade Kit containing DAPI from Molecular Probes (S36938, Life Technologies). Samples were examined with an epi-illumination microscope (DMI 6000, Leica) with a cooled charge-coupled device (CCD) camera (MicroMax, Princeton Instruments). Images were acquired with MetaMorph (Molecular Devices) and processed with MetaMorph and Photoshop CS2 (Adobe Systems Inc., San Jose, CA, USA).

Immunohistochemistry

Mature human kidney and 33-week-old fetal lung were embedded in OCT compound. Frozen sections, 8 μm-thick, were fixed in acetone for 10 minutes, treated with PBS containing 0.1% Tween 20, 3% BSA and 10% donkey serum for 1 hour and incubated in the same buffer overnight at 4℃ with appropriate antibodies. Hoechst (no. 33342, Sigma) was used to label the nuclei and slides were mounted with FLUOPREP (BioMerieux sa, Marcy L'Etoile, France). Light microscopy analyses of immunofluorescence samples were performed with an Epi-illumination microscope (DMI 6000, Leica Microsystems).

Eyes of a human adult donor [69-year-old female donor (hum252), 11.5 hours post-mortem] were cryofixed in melting isopentane and cryosectioned as described elsewhere (Wolfrum, 1992). Cryosections were placed on coverslips precoated with poly-L-lysine, and incubated with in PBS containing 0.01% Tween 20 for 20 minutes. After a PBS washing step, sections were covered with blocking solution (PBS containing 0.5% cold-water fish gelatin, 0.1% ovalbumin) and incubated for a minimum of 30 minutes followed by an overnight incubation with primary antibodies diluted in blocking solution at 4℃. Washed cryosections were incubated with secondary antibodies conjugated to Alexa Fluor 488 or Alexa Fluor 568 (Invitrogen) in PBS with DAPI (Sigma-Aldrich) for 1.5 hours at room temperature in the dark. After repeated washing with PBS, sections were mounted in Mowiol 4.88 (Hoechst). Light microscopy analyses of immunofluorescence samples were performed with a Leica DM6000 microscope (Leica microsystems).

Human eyes were obtained from the Dept. of Ophthalmology (Mainz, Germany) and kidney and lung samples from the Necker-Enfants Malades Hospital (Paris, France). Guidelines of the Declaration of Helsinki were followed.

Live-cell imaging and FRAP

Dynamics of SSTR3, SEPT2 and SEPT9 in the primary cilium were analyzed by live-cell fluorescence microscopy. RPE1 cells grown on μ-slides (Ibidi) were transfected with SSTR3-GFP- and/or SEPT9-tomato- or SEPT2-GFP and pericentrin-RFP-encoding plasmids in low serum media and analyzed 24 or 48 hours later. Live-cell fluorescence microscopy was performed using an Apo 100× NA 1.43 microscope objective and an inverted epi-illumination microscope (Axiovert 100 M, Zeiss) placed within a temperature-controlled enclosure set at 37℃. Images corresponding to GFP and tomato fluorescence were acquired successively every 3 seconds for 3–20 minutes. Shutters, filters, camera and acquisition were controlled by MetaMorph. The final movies and images were generated using ImageJ (http://rsbweb.nih.gov/ij/index.html) and Photoshop. Fluorescence recovery after photobleaching (FRAP) studies were performed with a laser scanning confocal microscope (TCS SP2 AOBS, Leica) after excitation with a 488-nm laser line from an argon laser, as described previously (Molla-Herman et al., 2010). Briefly, regions containing the primary cilium or another area of the same cells were exposed to two consecutive laser pulses of 1 second with 100% of the laser intensity, and recovery of fluorescence was analyzed for the indicated periods. Images were then analyzed using ImageJ to quantify normalized fluorescence in the selected zones. The fluorescence intensity at the photo-bleached regions was measured using ImageJ and the percentage of recovery was calculated as follows. In the first case, the whole cilium was photobleached and in the second case, only one half of the cilium was photobleached. The final images were generated using ImageJ and Photoshop (Adobe Systems Inc.).

Immunoprecipitation and immunoblotting

RPE cells were grown in the presence or absence of serum, extracted in buffer containing 10 mM Hepes–NaOH, pH 7.4, 140 mM KCl, 5 mM EGTA, 1 mM DTT, 2 mM Pefabloc, and 0.5% Triton X-100, and centrifuged at 20,000 ***g***. SEPT2–S-tag–GFP was immunoprecipitated from the resulting supernatant with a GFP antibody and protein-A–Sepharose 4B beads. The resulting immunoprecipitated proteins were treated with TEV protease, and processed for a second round of isolation with S-beads (Millipore). Following elution from the S-beads, proteins co-isolated with SEPT2 were separated by 10% SDS-PAGE and silver staining. Proteins were transferred onto Immobilon P membranes (Millipore), and incubated overnight at 4℃ in blocking buffer (10 mM Tris-HCl, pH 6.8, 150 mM NaCl, 1 mM DTT, 0.1% Tween 20, 2% BSA). SEPT9_v1, SEPT7 and SEPT2 antibodies were diluted in blocking buffer and incubated with the membrane for 2 hours. Blots were subsequently incubated with secondary Alexa-Fluor-680- and IRDye800-conjugated antibodies and scanned in a Li-COR infrared imager.

For immunoblotting, cells were lysed in lysis buffer [0.02 M Tris-HCl pH 7.5, 1% NP40, 0.1 M $(NH_4)_2SO_4$, 10% glycerol, 10 mM protease inhibitor cocktail (Sigma)] for 30 minutes at 4℃. After centrifugation, cleared lysates were separated by SDS-PAGE and transferred onto polyvinylidene fluoride transfer membranes (PVDF, GE Healthcare) using the NuPage electrophoresis system (Life technologies). Immunoblotting was performed using the indicated primary antibodies and revealed using the ECL$^+$ Detection Kit (GE Healthcare).

Statistical analysis

The percentage of ciliated cells and the length of primary cilium were quantified and measured using fluorescence microscope images and ImageJ. To determine the percentage of ciliated cells, we counted the number of nuclei (DAPI staining) in each image and the number of primary cilia detected by the AcTub staining. The percentage of ciliated cells was equal to (number of cilia/number of nuclei)×100. Cilia were measured with the analyze-measure option of ImageJ. All the results were then transferred to Excel. Student's *t*-tests and Fischer's tests were used for the percentage of ciliated cells and cilium length, respectively.

Acknowledgements

The authors thank all their generous collaborators for providing important reagents; Anthony Henneveu for his help with immunofluorescence and transfections; Flora Legendre for her help with immunohistochemistry; people from the 'Imagerie Cellulaire' facility of the Cochin Institute for their help; G. Pereira for sharing important new results; and A. Touré and N. Spassky for stimulating discussions.

Author contributions

R.G., Q.H., M.F., M.C.R. and B.S. performed and analyzed the experiments; S.M., U.W., S.S. and P.C. provided reagents, tissues samples, expertise and designed and analyzed some of the experiments; R.G., Q.H., W.J.N. and A.B. designed most of the experiments; W.J.N. and A.B. analyzed all the experiments; R.G., W.J.N. and A.B. wrote the manuscript; all the coauthors corrected the manuscript.

Funding

This work was supported by the National Institutes of Health [grant number GM35527 to W.J.N.]; a Department of Defense Breast Cancer Research Program Predoctoral Fellowship [grant number BC083077 to Q.H.]; Agence National de la Recherche [grant number R09087KS to A.B. and S.S.]; the Ministère de la Recherche et de l'Enseignement Supérieur [R.G.]; Région ile de France,

Cardiovasculaire Obésité-Rein-Diabète les domaines d'intérêt majeur (CORDDIM) [M.F.]; a Wellcome Trust Research Career Development Fellowship [grant number WT097411MA to S.M.]; a European Research Council Advanced Grant Award [grant number 233348 to S.M.]; and 'SYSCILIA' European Community's Seventh Framework Programme FP7/2009 [grant agreement number 241955 to U.W.]. Deposited in PMC for release after 6 months.

Supplementary material available online at
http://jcs.biologists.org/lookup/suppl/doi:10.1242/jcs.111377/-/DC1

References

Berbari, N. F., Johnson, A. D., Lewis, J. S., Askwith, C. C. and Mykytyn, K. (2008). Identification of ciliary localization sequences within the third intracellular loop of G protein-coupled receptors. *Mol. Biol. Cell* **19**, 1540-1547.

Bershteyn, M., Atwood, S. X., Woo, W.-M., Li, M. and Oro, A. E. (2010). MIM and cortactin antagonism regulates ciliogenesis and hedgehog signaling. *Dev. Cell* **19**, 270-283.

Chapin, S. J., Lue, C. M., Yu, M. T. and Bulinski, J. C. (1995). Differential expression of alternatively spliced forms of MAP4: a repertoire of structurally different microtubule-binding domains. *Biochemistry* **34**, 2289-2301.

Chih, B., Liu, P., Chinn, Y., Chalouni, C., Komuves, L. G., Hass, P. E., Sandoval, W. and Peterson, A. S. (2012). A ciliopathy complex at the transition zone protects the cilia as a privileged membrane domain. *Nat. Cell Biol.* **14**, 61-72.

Drewes, G., Ebneth, A., Preuss, U., Mandelkow, E. M. and Mandelkow, E. (1997). MARK, a novel family of protein kinases that phosphorylate microtubule-associated proteins and trigger microtubule disruption. *Cell* **89**, 297-308.

Estey, M. P., Di Ciano-Oliveira, C., Froese, C. D., Bejide, M. T. and Trimble, W. S. (2010). Distinct roles of septins in cytokinesis: SEPT9 mediates midbody abscission. *J. Cell Biol.* **191**, 741-749.

Francis, S. S., Sfakianos, J., Lo, B. and Mellman, I. (2011). A hierarchy of signals regulates entry of membrane proteins into the ciliary membrane domain in epithelial cells. *J. Cell Biol.* **193**, 219-233.

Garcia-Gonzalo, F. R., Corbit, K. C., Sirerol-Piquer, M. S., Ramaswami, G., Otto, E. A., Noriega, T. R., Seol, A. D., Robinson, J. F., Bennett, C. L., Josifova, D. J. et al. (2011). A transition zone complex regulates mammalian ciliogenesis and ciliary membrane composition. *Nat. Genet.* **43**, 776-784.

Gilula, N. B. and Satir, P. (1972). The ciliary necklace. A ciliary membrane specialization. *J. Cell Biol.* **53**, 494-509.

Händel, M., Schulz, S., Stanarius, A., Schreff, M., Erdtmann-Vourliotis, M., Schmidt, H., Wolf, G. and Höllt, V. (1999). Selective targeting of somatostatin receptor 3 to neuronal cilia. *Neuroscience* **89**, 909-926.

Hildebrandt, F., Benzing, T. and Katsanis, N. (2011). Ciliopathies. *N. Engl. J. Med.* **364**, 1533-1543.

Holmfeldt, P., Brattsand, G. and Gullberg, M. (2002). MAP4 counteracts microtubule catastrophe promotion but not tubulin-sequestering activity in intact cells. *Curr. Biol.* **12**, 1034-1039.

Holmfeldt, P., Stenmark, S. and Gullberg, M. (2007). Interphase-specific phosphorylation-mediated regulation of tubulin dimer partitioning in human cells. *Mol. Biol. Cell* **18**, 1909-1917.

Holmfeldt, P., Sellin, M. E. and Gullberg, M. (2009). Predominant regulators of tubulin monomer-polymer partitioning and their implication for cell polarization. *Cell. Mol. Life Sci.* **66**, 3263-3276.

Hsu, S. C., Hazuka, C. D., Roth, R., Foletti, D. L., Heuser, J. and Scheller, R. H. (1998). Subunit composition, protein interactions, and structures of the mammalian brain sec6/8 complex and septin filaments. *Neuron* **20**, 1111-1122.

Hu, Q. and Nelson, W. J. (2011). Ciliary diffusion barrier: the gatekeeper for the primary cilium compartment. *Cytoskeleton (Hoboken)* **68**, 313-324.

Hu, Q., Nelson, W. J. and Spiliotis, E. T. (2008). Forchlorfenuron alters mammalian septin assembly, organization, and dynamics. *J. Biol. Chem.* **283**, 29563-29571.

Hu, Q., Milenkovic, L., Jin, H., Scott, M. P., Nachury, M. V., Spiliotis, E. T. and Nelson, W. J. (2010). A septin diffusion barrier at the base of the primary cilium maintains ciliary membrane protein distribution. *Science* **329**, 436-439.

Ihara, M., Kinoshita, A., Yamada, S., Tanaka, H., Tanigaki, A., Kitano, A., Goto, M., Okubo, K., Nishiyama, H., Ogawa, O. et al. (2005). Cortical organization by the septin cytoskeleton is essential for structural and mechanical integrity of mammalian spermatozoa. *Dev. Cell* **8**, 343-352.

Ishikawa, H. and Marshall, W. F. (2011). Ciliogenesis: building the cell's antenna. *Nat. Rev. Mol. Cell Biol.* **12**, 222-234.

Ishikawa, H., Thompson, J., Yates, J. R., 3rd and Marshall, W. F. (2012). Proteomic analysis of mammalian primary cilia. *Curr. Biol.* **22**, 414-419.

Joo, E., Surka, M. C. and Trimble, W. S. (2007). Mammalian SEPT2 is required for scaffolding nonmuscle myosin II and its kinases. *Dev. Cell* **13**, 677-690.

Kim, J., Lee, J. E., Heynen-Genel, S., Suyama, E., Ono, K., Lee, K., Ideker, T., Aza-Blanc, P. and Gleeson, J. G. (2010a). Functional genomic screen for modulators of ciliogenesis and cilium length. *Nature* **464**, 1048-1051.

Kim, S. K., Shindo, A., Park, T. J., Oh, E. C., Ghosh, S., Gray, R. S., Lewis, R. A., Johnson, C. A., Attie-Bittach, T., Katsanis, N. et al. (2010b). Planar cell polarity acts through septins to control collective cell movement and ciliogenesis. *Science* **329**, 1337-1340.

Kim, M. S., Froese, C. D., Estey, M. P. and Trimble, W. S. (2011). SEPT9 occupies the terminal positions in septin octamers and mediates polymerization-dependent functions in abscission. *J. Cell Biol.* **195**, 815-826.

Kinoshita, M., Field, C. M., Coughlin, M. L., Straight, A. F. and Mitchison, T. J. (2002). Self- and actin-templated assembly of Mammalian septins. *Dev. Cell* **3**, 791-802.

Kissel, H., Georgescu, M.-M., Larisch, S., Manova, K., Hunnicutt, G. R. and Steller, H. (2005). The Sept4 septin locus is required for sperm terminal differentiation in mice. *Dev. Cell* **8**, 353-364.

Kremer, B. E., Haystead, T. and Macara, I. G. (2005). Mammalian septins regulate microtubule stability through interaction with the microtubule-binding protein MAP4. *Mol. Biol. Cell* **16**, 4648-4659.

Kuhns, S., Schmidt, K. N., Reymann, J., Gilbert, D. F., Neuner, A., Hub, B., Carvalho, R., Wiedemann, P., Zentgraf, H., Erfle, H. et al. (2013). The microtubule affinity regulating kinase MARK4 promotes axoneme extension during early ciliogenesis. *J. Cell Biol.* **200**, 505-522.

Liu, Q., Tan, G., Levenkova, N., Li, T., Pugh, E. N., Jr, Rux, J. J., Speicher, D. W. and Pierce, E. A. (2007). The proteome of the mouse photoreceptor sensory cilium complex. *Mol. Cell. Proteomics* **6**, 1299-1317.

Mayer, U., Küller, A., Daiber, P. C., Neudorf, I., Warnken, U., Schnölzer, M., Frings, S. and Möhrlen, F. (2009). The proteome of rat olfactory sensory cilia. *Proteomics* **9**, 322-334.

Molla-Herman, A., Ghossoub, R., Blisnick, T., Meunier, A., Serres, C., Silbermann, F., Emmerson, C., Romeo, K., Bourdoncle, P., Schmitt, A. et al. (2010). The ciliary pocket: an endocytic membrane domain at the base of primary and motile cilia. *J. Cell Sci.* **123**, 1785-1795.

Mostowy, S. and Cossart, P. (2012). Septins: the fourth component of the cytoskeleton. *Nat. Rev. Mol. Cell Biol.* **13**, 183-194.

Mostowy, S., Nam Tham, T., Danckaert, A., Guadagnini, S., Boisson-Dupuis, S., Pizarro-Cerdá, J. and Cossart, P. (2009). Septins regulate bacterial entry into host cells. *PLoS ONE* **4**, e4196.

Mostowy, S., Bonazzi, M., Hamon, M. A., Tham, T. N., Mallet, A., Lelek, M., Gouin, E., Demangel, C., Brosch, R., Zimmer, C. et al. (2010). Entrapment of intracytosolic bacteria by septin cage-like structures. *Cell Host Microbe* **8**, 433-444.

Narita, K., Kozuka-Hata, H., Nonami, Y., Ao-Kondo, H., Suzuki, T., Nakamura, H., Yamakawa, K., Oyama, M., Inoue, T. and Takeda, S. (2012). Proteomic analysis of multiple primary cilia reveals a novel mode of ciliary development in mammals. *Biol. Open* **1**, 815-825.

Nguyen, H. L., Chari, S., Gruber, D., Lue, C. M., Chapin, S. J. and Bulinski, J. C. (1997). Overexpression of full- or partial-length MAP4 stabilizes microtubules and alters cell growth. *J. Cell Sci.* **110**, 281-294.

Nguyen, H. L., Gruber, D. and Bulinski, J. C. (1999). Microtubule-associated protein 4 (MAP4) regulates assembly, protomer-polymer partitioning and synthesis of tubulin in cultured cells. *J. Cell Sci.* **112**, 1813-1824.

Oegema, K., Savoian, M. S., Mitchison, T. J. and Field, C. M. (2000). Functional analysis of a human homologue of the Drosophila actin binding protein anillin suggests a role in cytokinesis. *J. Cell Biol.* **150**, 539-552.

Pedersen, L. B. and Rosenbaum, J. L. (2008). Intraflagellar transport (IFT) role in ciliary assembly, resorption and signalling. *Curr. Top. Dev. Biol.* **85**, 23-61.

Perez, F., Diamantopoulos, G. S., Stalder, R. and Kreis, T. E. (1999). CLIP-170 highlights growing microtubule ends in vivo. *Cell* **96**, 517-527.

Pitaval, A., Tseng, Q., Bornens, M. and Théry, M. (2010). Cell shape and contractility regulate ciliogenesis in cell cycle-arrested cells. *J. Cell Biol.* **191**, 303-312.

Saarikangas, J. and Barral, Y. (2011). The emerging functions of septins in metazoans. *EMBO Rep.* **12**, 1118-1126.

Sellin, M. E., Sandblad, L., Stenmark, S. and Gullberg, M. (2011). Deciphering the rules governing assembly order of mammalian septin complexes. *Mol. Biol. Cell* **22**, 3152-3164.

Sharma, N., Kosan, Z. A., Stallworth, J. E., Berbari, N. F. and Yoder, B. K. (2011). Soluble levels of cytosolic tubulin regulate ciliary length control. *Mol. Biol. Cell* **22**, 806-816.

Spiliotis, E. T. (2010). Regulation of microtubule organization and functions by septin GTPases. *Cytoskeleton (Hoboken)* **67**, 339-345.

Spiliotis, E. T., Hunt, S. J., Hu, Q., Kinoshita, M. and Nelson, W. J. (2008). Epithelial polarity requires septin coupling of vesicle transport to polyglutamylated microtubules. *J. Cell Biol.* **180**, 295-303.

Thomas, J., Morlé, L., Soulavie, F., Laurençon, A., Sagnol, S. and Durand, B. (2010). Transcriptional control of genes involved in ciliogenesis: a first step in making cilia. *Biol. Cell* **102**, 499-513.

Tooley, A. J., Gilden, J., Jacobelli, J., Beemiller, P., Trimble, W. S., Kinoshita, M. and Krummel, M. F. (2009). Amoeboid T lymphocytes require the septin cytoskeleton for cortical integrity and persistent motility. *Nat. Cell Biol.* **11**, 17-26.

Trinczek, B., Brajenovic, M., Ebneth, A. and Drewes, G. (2004). MARK4 is a novel microtubule-associated proteins/microtubule affinity-regulating kinase that binds to the cellular microtubule network and to centrosomes. *J. Biol. Chem.* **279**, 5915-5923.

Trojan, P., Krauss, N., Choe, H.-W., Giessl, A., Pulvermüller, A. and Wolfrum, U. (2008). Centrins in retinal photoreceptor cells: regulators in the connecting cilium. *Prog. Retin. Eye Res.* **27**, 237-259.

Wolfrum, U. (1992). Cytoskeletal elements in arthropod sensilla and mammalian photoreceptors. *Biol. Cell* **76**, 373-381.